Combustion and Flame 176 (2017) 60–71

Contents lists available at ScienceDirect

Combustion and Flame

journal homepage: www.elsevier.com/locate/combustflame

A molecular dynamics investigation of n-alkanes vaporizing into nitrogen: transition from subcritical to supercritical

Guiyuan Mo, Li Qiao*

School of Aeronautics and Astronautics, Purdue University, West Lafayette, IN 47907, United States

ARTICLE INFO

Article history:
Received 8 February 2016
Revised 18 March 2016
Accepted 28 September 2016

Keywords:
Supercritical evaporation
Hydrocarbon fuels
Molecular dynamics simulations
Transition from subcritical to supercritical

ABSTRACT

The injection, evaporation and mixing processes of hydrocarbon fuels into a supercritical environment are not yet well understood. The present paper investigated evaporation of three n-alkane fuels into nitrogen under various temperatures and pressures by molecular dynamics simulations. The emphasis was to understand at what conditions, when and how the transition from classical two-phase evaporation to one-phase diffusion-controlled mixing takes place. The reduced ambient temperature and pressure range from 0.8 to 2.4 and 0.55 to 14.3, respectively. Scaling law was explored with hopes to extend the conclusions to macroscopic systems. The dimensionless transition time from subcritical to supercritical (with respect to the liquid lifetime) was found to be independent of liquid film thickness, but it has strong dependence on ambient temperature and pressure. With higher ambient temperature and pressure, the transition occurs earlier in the liquid's lifetime. Correlations for dimensionless transition time were proposed to describe such dependence. Additionally, a threshold dimensionless transition time of 0.35 may be used to separate the subcritical-dominated regime and the supercritical-dominated regime on the P-T diagram. Lastly, the normalized liquid lifetime (by a reference lifetime and the film thickness) depends only on the ambient temperature and pressure. As pressure increases, it decreases for subcritical-dominated cases mainly because the enthalpy of vaporization reduces with increasing pressure. The trend, however, is reversed for supercritical-dominated cases where the liquid lifetime increases slightly with increasing pressure.

1. Introduction

Practical engines such as liquid rockets and diesel engines operate at high pressures. As a result, the injected fuel may be at transcritical or supercritical state during the injection, mixing and vaporization processes. Several reviews [1–3] have provided important insights on supercritical behaviors, as well as limitations of current theoretical modeling and numerical simulations of such behaviors. The introduction of thermodynamic nonidealities and transport anomalies near the critical point is one of the main challenges to model these phenomena. Very limited experimental data are available for either quantitative understanding of the physics or for assessment of various models. Although we have good knowledge of the classical two-phase atomization regime and the supercritical one-phase mixing regime, the transition from the former to the latter is less understood. One of the key questions is this: for a specific fuel, single or multi-component, under what conditions the evaporation and mixing processes are subcritical in nature and under what conditions they become supercritical. There are inconsistent answers to this question between experiments and modeling/simulations in the literature.

Several high-pressure injection experiments have demonstrated that supercritical mixing can be observed at pressures near or slightly higher than the critical pressure of the liquid fuel [4–8]. For example, Mayer and Schik [4] stated "when the chamber pressure approaches the critical pressure, injection can no longer be regarded as simple spray formation, but rather as a fluid/fluid mixing process that can be very sensitive to smaller perturbations in pressure, temperature, and local mixture composition." Segal and Polikhov [5] observed transitional mixing when the experimental conditions were in the vicinity of the critical point of the liquid fuel; both droplet formation and irregularly shaped material broke from the injectant were observed. Chehroudi et al. [7] showed that when the chamber pressure was at or above the critical pressure of the injectant, the classical liquid jet breakup phenomena disappeared and gas-like jet behavior emerged. Oschwald et al. [8] observed major structural changes of the jet at the interface at a reduced pressure of 1.03 (from classical drops to irregular finger-like entities).

Recent experiments done at Sandia National Lab [9,10] focused on the transition from classical droplet evaporation to miscible

* Corresponding author.
E-mail address: lqiao@purdue.edu (L. Qiao).

http://dx.doi.org/10.1016/j.combustflame.2016.09.028
0010-2180/

fluid mixing. Especially, the time evolution of the transition from liquid droplet to fuel vapor was captured at the microscopic level using a high-speed camera along with a long-distance microscope. The experimental observations show that when the ambient pressure is above 64–70 atm at $T = 1000$ K, n-heptane, n-dodecane and n-hexadecane all exhibit significant miscible mixing behavior, implying that at these conditions the evaporation has become diffusion-dominated mixing process.

However, previous modeling studies [11–14] have suggested for the same or similar fuel the minimum pressure required for a transition from subcritical to supercritical to occur is in the range of 90–109 atm at $T = 1000$ K. For example, Oefelein and Aggarwal [11] developed a unified high-pressure drop vaporization model for use in numerical simulations of high-pressure spray combustion processes. With this model, they performed direct numerical simulations (DNS) to simulate the transient process of n-hexane droplets vaporizing into nitrogen. The results show that the minimum pressure required for a 100-μm n-hexane droplet to attain the critical mixing state at the droplet surface is approximately 98 atm at an ambient temperature of 1000 K. Zhu et al. [12] simulated an n-heptane droplet vaporizing into nitrogen and reported the minimum pressure required for the droplet to attain its critical mixing state is about 109 atm at 1000 K. Zhu et al. later [13] simulated the transient supercritical droplet evaporation of millimeter-sized n-heptane droplets and found that at 1000 K the minimum pressure is 90 and 109 atm using the quasi-steady and transient models, respectively. Additionally, Zhu & Reitz [14] modeled and compared the evaporation behavior of diesel fuel and a single-component diesel surrogate fuel (n-tridecane), showing the minimum pressure required for transition from subcritical to supercritical for the two fuels is 123 and 104 atm, respectively, at 1000 K.

To summarize, for a specific fuel the minimum pressure required for transition to occur reported by the modeling studies are higher than those observed in the experiments. The reason for such deviation is very complex. One possibility is that when the mixture at the interface is approaching its critical mixing state, the thermodynamic and transport properties become very sensitive to small perturbations and are hard to model. For example, the way we currently model transport properties at high pressures is based on the kinetic theory for idea gases with a correction term to account for high-pressure effect; critical enhancement is usually neglected [1]. Underestimation of the thermodynamic and transport properties may result in a higher minimum pressure required for transition to occur.

Dahms and Oefelein [15–18] have recently made important contributions on understanding the transition from classical spray regime to supercritical diffusion-controlled mixing regime. They used a real-fluid model, combined with Linear Gradient Theory, to model the gas/liquid interface structure, based on which they proposed a criteria (using a threshold Knudsen number of 0.1) to separate the classical spray regime and the diffusion-dominated mixing regime on a P-T diagram. These analyses provide important insights on which regime practical engines such as rockets, gasoline and diesel engines fall into based on their operation conditions. Nevertheless, the thermodynamic analysis of the interface is under the assumption of steady-state, which does not reflect the dynamic process of a liquid when exposed to a high-temperature and pressure environment. In other words, when a cold liquid fuel is injected into a combustion chamber, the transition does not take place instantaneously. Surface tension will exist at first. After some time, the liquid will experience a transition to supercritical mixing. The Knudsen number of the interface is continuously changing during the evaporation and mixing processes. More quantitative studies are required to understand the transition, e.g., how does it depend on fuel type, ambient pressure and temperature.

Motivated by all of the above, we chose a different approach – molecular dynamics (MD) simulations to understand when and how a transition from classical evaporation to supercritical mixing takes place when a cold liquid fuel is placed in a hot high-pressure environment. Continuum based methods enable large scale simulations and are essential for predicting the combustion processes in practical engines. However, the challenge lies in the fact that there are large uncertainties in thermodynamic and transport properties at high pressures, especially for complex mixtures near the critical state [16]. MD simulations are computationally costly and usually limited to small scales (a few to a few hundred nanometers). However, the advantage of MD is that no assumptions are made about the processes or physics to be investigated. The only input is a potential model that describes intermolecular interaction. Models for Equation of State, mixing rules, thermodynamic and transport properties are not required. Equilibrium at vapor/liquid interface is not assumed. From this perspective, a molecular approach can be valuable by understanding fundamental physics, examining assumptions, and providing empirical parameters for phenomenological models. This will complement continuum-based approaches to enable more accurate simulations of the disintegration and combustion processes of a liquid jet in high-pressure propulsion systems.

Previous MD studies [19–37] of droplet evaporation focused mostly on subcritical conditions. Kaltz et al. [26] are among the first to investigate supercritical behaviors using a molecular approach. They simulated the evaporation of liquid oxygen into gaseous hydrogen or helium at various temperatures and pressures using the L-J 12-6 potential. The results show that droplets retained a spherical geometry with a distinct temperature profile throughout the entire vaporization process at subcritical conditions. At supercritical conditions, however, the drops quickly lost their spherical shape and became more cloud shaped and the surface tension soon disappeared. Significant concentration of the gas phase species was dissolved in the droplet at moderate- and high-ambient pressures. Most MD simulations chose simple fluids, such as argon, helium, xenon, and oxygen, so the intermolecular potential can be expressed by the simple L-J potential. Few have considered large molecules such as hydrocarbon fuels at high pressures, especially the transition from subcritical to supercritical, for which there is a knowledge gap.

The present paper investigated evaporation of n-heptane, n-dodecane and n-hexadecane into nitrogen environment under various ambient pressures and temperatures via MD simulations. The reduced ambient temperature (T/T_c) ranged from 0.8 to 2.4, and the reduced ambient pressure (P/P_c) ranged from 0.55 to 14.3, both of which cover the relevant operating conditions of liquid rockets. The emphasis is to understand at what conditions, when and how a transition from subcritical to supercritical takes place. After introducing the method of molecular dynamics simulations, the paper describes the main features of subcritical evaporation, supercritical evaporation, and the scaling law. A dimensionless transition time is introduced and its dependence on fuel type, ambient temperature and pressure is discussed. Then the criterion for transition to occur is proposed. Lastly, the dependence of the liquid life time on ambient temperature and pressure is discussed.

2. Molecular dynamics simulations

2.1. Interatomic potentials

Molecular models for hydrocarbons can be divided into two categories: all-atom (AA) models and united-atom (UA) models. The former treat each atom as one site, whereas the latter treat each CH_3 and CH_2 as one site to improve computational efficiency. Four UA models are commonly used for hydrocarbons, including TraPPE

by Martin and Siepmann [38], SKS by Smit et al. [39], NERD by Nath et al. [40], and OPLS-UA by Jorgensen et al. [41]. For nitrogen, two models are typically used – central LJ potential and two-center LJ potential.

The authors [42] have recently employed different UA models to compute the vapor–liquid equilibrium (VLE) diagram for n-alkane (C_7–C_{16}) and nitrogen mixtures by configurational-bias Monte Carlo (MC) simulations combined with Gibbs ensembles. The MC predictions were compared to the experimental data [43]. The comparison demonstrated that SKS (for alkanes) coupled with a Rivera 2002 model (for nitrogen) [44] performs best in predicting the vapor–liquid equilibrium of n-alkane/nitrogen mixtures, even at pressures as high as 20 MPa. The deviation between predictions and measured data is smaller at higher temperatures. When temperature is greater than 411 K, the deviation is less than 5% for all pressures in the range of 1 MPa to 20 MPa. Based on this comparison, the SKS model was chosen for alkanes, and the two-center L-J model Rivera 2002 [44] was chosen for nitrogen to simulate the evaporation process of alkanes into nitrogen at various temperatures and pressures.

The interaction between atoms in different molecules and the atoms in the same molecule but apart more than three bonds away is modeled by truncated Lennard-Jones (L-J) 6-12 potential, which has been widely used in molecular simulations:

$$U_{LJ}(r_{ij}) = 4\varepsilon_{ij}\left[\left(\frac{\sigma_{ij}}{r_{ij}}\right)^{12} - \left(\frac{\sigma_{ij}}{r_{ij}}\right)^{6}\right] \quad (1)$$

where r_{ij} is the interatomic distance, ε_{ij} and σ_{ij} are the interaction potential well depth and the zero-energy separation distance for atom pair i and j. Lorentz-Berthelot combining rule was used to find appropriated L-J parameters for interactions between unlike molecules [45]:

$$\varepsilon_{ij} = \sqrt{\varepsilon_i \times \varepsilon_j} \quad \sigma_{ij} = (\sigma_i + \sigma_j)/2 \quad (2)$$

The original SKS model treats all bonds as rigid with a fixed length of 1.53 Å. However, the LAMMPS platform [46] does not allow bond constraints for large molecules. So a harmonic potential is used for bond stretching to replace the rigid bond in the original SKS model:

$$U(r) = \frac{k_r}{2}(r - r_0)^2 \quad (3)$$

where r_0 is the bond length of 1.53 Å. k_r is set to be 191.77 Kcal/(mol*Å^2) as parameterized in the NERD model [40]. We compared the evaporation characteristics by using rigid bond with a fixed length (performed on GROMACS platform with LINCS constraint algorithms [47]) and using harmonic potential for bond stretching (performed on LAMMPS platform [46]). No difference was observed and therefore this modified SKS model was used on LAMMPS for the present work.

Bond-angle bending is governed by a harmonic potential:

$$U(\theta) = \frac{k_\theta}{2}(\theta - \theta_0)^2 \quad (4)$$

where θ is the bond angle between three consecutive united atoms. The dihedral angles are governed by the torsion potential as a Fourier series:

$$U(\phi) = c_1(1 + \cos\phi) + c_2(1 - \cos 2\phi) + c_3(1 + \cos 3\phi) \quad (5)$$

where ϕ is the dihedral angle between four consecutive united atoms. The nitrogen model proposed by Rivera et al. [44] also assumes that the bond length is fixed. The parameters in these models are summarized in Table 1.

Table 1
Parameters for SKS and Rivera models.

		SKS	Rivera
Nonbonded	ε/k_b(K)	CH_3: 114 CH_2: 47	36
	σ (Å)	CH_3: 3.93 CH_2: 3.93	3.31
Bond	r_0 (Å)	1.53	1.0897
Angle	θ_0	114°	
	k_θ/k_b (K/rad^2)	62,500	
Torsion	c_1/k_b (K)	355.03	
	c_2/k_b (K)	−68.19	
	c_3/k_b (K)	791.32	

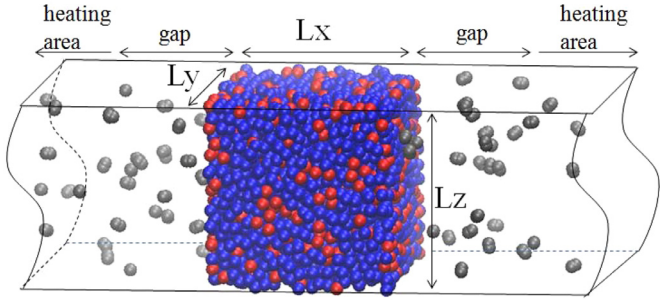

Fig. 1. Configuration of the simulation box. Atoms: red (CH_3), blue (CH_2), grey (N). (For interpretation of the references to color in this figure legend, the reader is referred to the web version of this article.)

2.2. Simulation configurations

Figure 1 shows the rectangular simulation box with periodic boundary conditions at both ends. The center of the box is filled with liquid n-heptane, n-dodecane or n-hexadecane, which is surrounded by nitrogen gas on two sides. The box has a fixed cross section of $L_y \times L_z = 5 \times 5$ nm for all simulations. The film thickness L_x, however, is varied (10 and 20 nm), corresponding to 600 and 1200 n-dodecane molecules, respectively. The liquid has an initial temperature of 363 K. The ambient temperature and pressure of nitrogen are varied to understand their effects on evaporation. NVT ensembles – constant atom number (N), constant volume (V), and constant temperature (T) – were used for the ambient gas nitrogen.

The number of nitrogen molecules in the simulation box must be large enough so that the pressure increase due to the addition of vaporized alkanes molecules into the ambient gas is negligible. Therefore constant pressure of the ambient gas can be assumed during the evaporation. For all the instances under various ambient temperatures and pressures, we found that when the ratio of number of atoms of ambient gas to the number of atoms of liquid is larger than 1, the evaporation characteristics become independent of the ratio, as shown in Fig. 2. As such, we chose an atom ratio of 5 for all the simulations. Therefore, the length of the entire simulation box ranges from 180 to 5200 nm, depending on the ambient temperature and pressure. Each simulation was run using 6 nodes with each node having 16 processors (Intel Xeon-E5) and 64 GB memory. The wall clock time for the simulation which contains 1200 n-dodecane molecules and 36,000 nitrogen molecules is about 280 hours. A total of 210 simulations were performed.

2.3. Ambient conditions

The ambient gas remains a constant temperature and pressure during a simulation. It provides heat to the liquid for vaporization. Because of that, the velocities of the molecules in this region are rescaled constantly to ensure a constant temperature. A gap between the liquid film and the heating area with a size of about

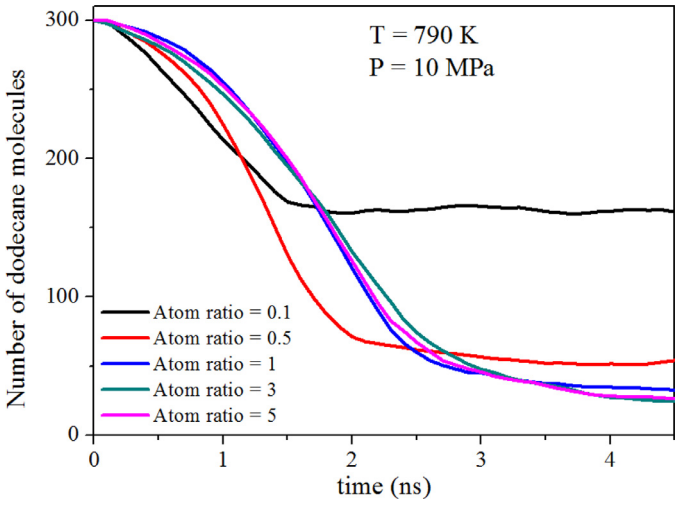

Fig. 2. Effect of atom ratio (the number of atoms in nitrogen to the number of atoms in n-dodecane) on evaporation characteristics.

50σ (σ is nitrogen molecule diameter) is required to minimize the effect of the heating boundary on the liquid-surface dynamics, as illustrated in Fig. 1. Before modeling evaporation, the initial configurations for the liquid and the ambient gas are equilibrated separately and then combined by placing the equilibrated liquid in an equilibrated environment of nitrogen. The equilibrated liquid is prepared by equilibrium with its own vapor at the initial liquid temperature using NVT ensemble. The reduced ambient temperature (T/T_c) and pressure (P/P_c) studied in this work range from 0.8 to 2.4 and 0.55 to 14.3, respectively.

2.4. Property measurement

MD simulations were carried out using the LAMMPS software platform [46]. The equations of atom motion were integrated by Verlet algorithm [45]. The time step was 2 fs. The atom initial velocity was assigned randomly according to Gaussian distribution. After running several test cases with different initial velocity, we found that the simulation results were independent of the initial velocity assignment. To obtain the spatial distribution of thermodynamic properties, such as density, mole fraction, temperature, and pressure–tensor, the simulation system was divided into slabs along the *X*-direction and averaged over 50 picoseconds statistically in each slab. The sizes of each slab along *X*, *Y*, and *Z* directions were d*x*, L_y, and L_z, respectively. A value of 0.2 nm was chosen for d*x*. The temperature can be calculated by averaged kinetic energy using the following equation:

$$\frac{3}{2}k_bTN = \sum_{i=1}^{N}\frac{1}{2}m_iv_i^2 \tag{6}$$

where N is the number of atoms in each slab, m_i and v_i are the ith atom's mass and velocity, respectively. The Boltzmann constant is k_b. The system pressure was obtained by

$$P = \frac{Nk_bT}{V} + \left(\sum_{i=1}^{N} r_iF_i\right)/dV \tag{7}$$

The first term on the right-hand side is the kinetic energy tensor, and the second term is the virial tensor. Here r_i is the radius-vector of the ith particle; F_i is the force acting on the particle; V is the volume of the system; and d is the dimension ($d = 3$).

Surface tension of a liquid results from the attractive force exerted on the surface molecules of the liquid. The molecules on the gas/liquid interface region experience a net attraction force toward the liquid phase because the interaction between liquid molecules are much stronger than between gas molecules. The integrated difference between the normal and tangential pressure-tensors is the surface tension of the liquid. The surface tension was calculated according to the Irving and Kirkwood method [48] by:

$$\gamma = 0.5\int_{-\infty}^{\infty}(p_n(x) - p_t(x))dx \tag{8}$$

where the normal pressure–tensor $p_n(x)=p_{XX}(x)$ and the tangential pressure–tensor $p_t(x)=(p_{YY}(x)+p_{ZZ}(x))/2$. The factor 0.5 in Eq. (8) is because two interfaces of the liquid film were counted. The x-dependent tangential pressure tensor can be computed by considering the kinetic term and potential term as [45]:

$$p_t(x) = \langle\rho(x)\rangle k_bT - \frac{1}{2A}\left\langle\sum_{i=1}^{N-1}\sum_{j>i}^{N}\frac{\left(y_{ij}^2+z_{ij}^2\right)}{2r_{ij}}U'_{LJ}\left(r_{ij}\right)\right.$$
$$\left.\times\frac{1}{|x_{ij}|}\theta\left(\frac{x-x_i}{x_{ij}}\right)\theta\left(\frac{x_j-x}{x_{ij}}\right)\right\rangle \tag{9}$$

where $\rho(x)$ is the density spatial distribution along x direction; $A = L_y \times L_z$ is the cross section area; x_{ij}, y_{ij} and z_{ij} is the distance between particle i and j in x, y, and z direction, respectively; r_{ij} is the total distance; $\theta(v)$ is the unit step function which is equal to 0 when $v < 0$ and 1 when $v \geq 0$; $\langle\ldots\rangle$ represents canonical ensemble average. The distance of x_{ij} is divided into N_s slabs with a thickness of dx. Each slab obtains equal contribution of $1/N_s$ from the particle i and j interaction if the straight line connecting particle i and j crosses, starts or ends in the slab. The normal component $p_n(x)$ can be calculated by replacing $(y_{ij}^2+z_{ij}^2)/2$ with x_{ij}^2 in Eq. (9).

3. Results and discussion

3.1. Subcritical evaporation

The main purpose of looking into subcritical evaporation is to provide a baseline for understanding supercritical behaviors. For the example discussed below, the ambient temperature and pressure are 526 K and 1 MPa, respectively. The initial liquid film thickness $L_x = 10$ nm. Note that the critical temperature and pressure of n-dodecane are 658 K and 1.817 MPa. The liquid fuel has an initial temperature of 363 K.

It is well-known that at subcritical conditions a distinctive interface exists, which separates the liquid core and the ambient gases. Figure 3 presents the evolution of the interface during the evaporation process. Figure 3(a) shows the spatial distribution of temperature and n-dodecane mole fraction at $t = 5$ ns. At a fixed time t during the evaporation process, the mole fraction value at a specific location corresponds to a certain value of temperature. Therefore a correlation between temperature and n-dodecane mole fraction can be obtained for each time t, as plotted in Fig. 3(b). In this figure, the vapor–liquid equilibrium (VLE) diagram for n-dodecane/nitrogen mixture at 1 MPa was obtained from the experimental data of Cordova et al. [43]. The left curve is the liquid phase equilibrium line; the right one is the gas phase equilibrium line. The two intersections resulting from the VLE lines and the temperature lines define the gas–liquid interface. The intersection with the VLE liquid phase line defines the inner boundary of the interface (close to the liquid core); the VLE gas phase defines the outer boundary (close to the ambient gas), as plotted in Fig. 3(b). The area between the two intersections marks the interface area where gas and liquid are at equilibrium. On the left side of the interface region, only gas presents; on the right side of the interface region, only liquid presents. It is clear that the temperature of the liquid core and the interface can never increase beyond the critical mixing temperature (the merge point of the two VLE lines, which,

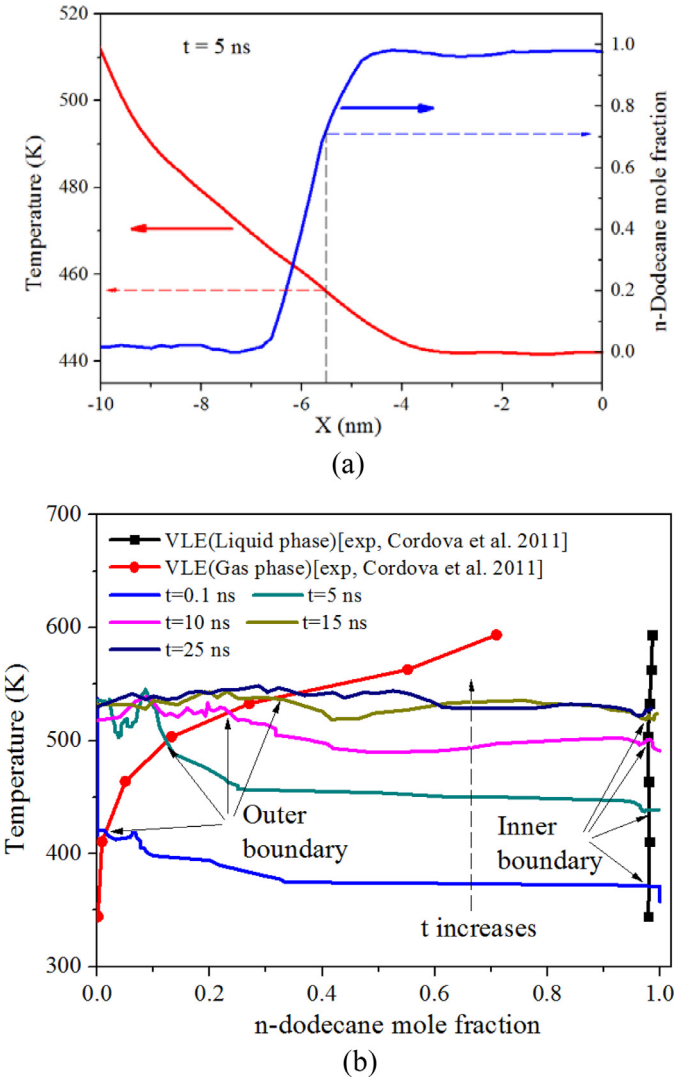

Fig. 3. (a) The spatial distribution profiles of temperature and n-dodecane mole fraction at $t = 5$ ns. (b) The development of gas–liquid interface on the temperature – mole fraction VLE diagram at 1 MPa (VLE exp data: [43]).

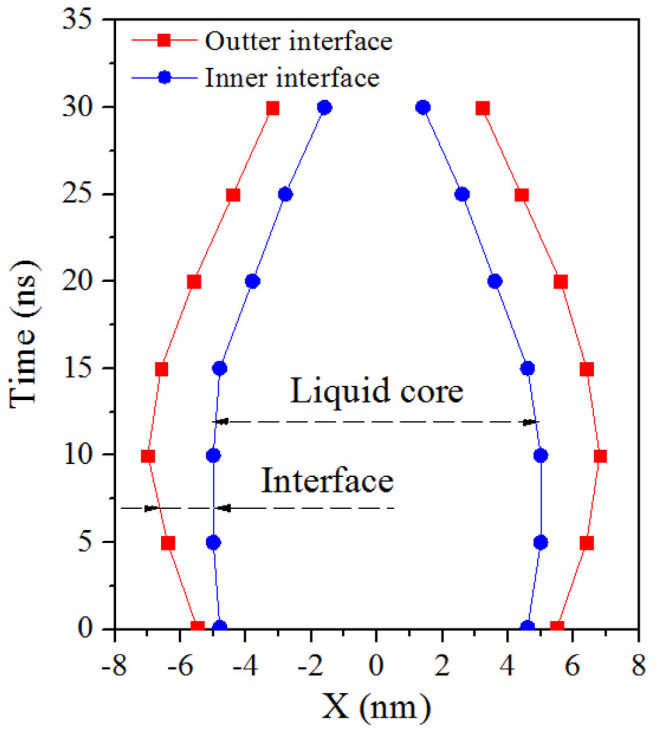

Fig. 4. The evolution of the gas/liquid interface during the evaporation process.

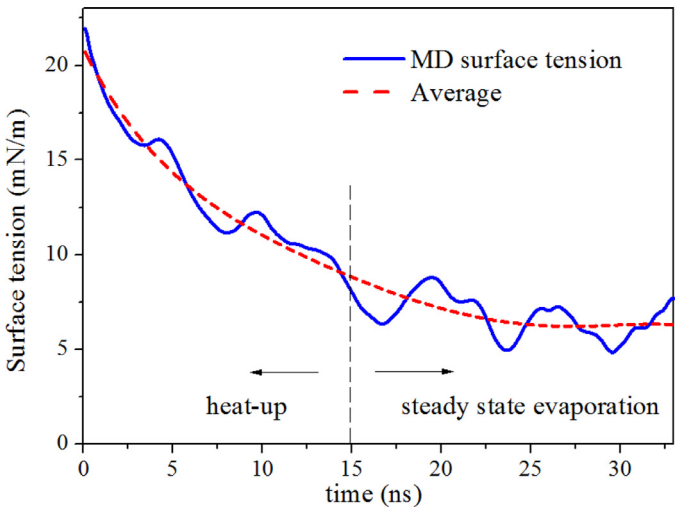

Fig. 5. The variation of the surface tension as a function of time.

however, is not shown by the experimental data). The liquid core and the interface are retained until the end of evaporation. Furthermore, n-dodecane mole fraction at the inner boundary of the interface remains unchanged, nearly 98%. However, at the outer boundary of the interface, the mole fraction of n-dodecane continues to increase over time.

The location of the interface (inner and outer boundaries) can be determined as a function of time during the evaporation process; the results are shown in Fig. 4. The liquid core can be seen to swell slightly during the heat-up period and then regress linearly during the steady-state evaporation stage. The thickness of the interface increases during the heat-up stage and then remains constant during the steady-state stage (about 2 nm). This number is consistent with the predictions of Dahms and Oefelein [17], who found the thickness of the interface at equilibrium varies from 0.9 to 2.6 nm under various temperatures and pressures.

Figure 5 shows the surface tension history during the evaporation process. At the beginning ($t = 0$ ns), the calculated surface tension is 21.9 mN/m, close to the experimental value of 19.2 mN/m (at 363 K) for n-dodecane in its own vapor [49]. Note that results from MD simulations often exhibit an oscillation nature, which is not surprising because the physical properties are extracted statistically and the number of molecules MD can simulate is limited. The dashed line shows the averaged value. The surface tension decreases during the heat-up stage because the temperature of the liquid core increases. When it enters steady-state evaporation, the surface tension keeps nearly constant.

During the entire evaporation process, n-dodecane mole fraction in the liquid core is close to 1. The liquid core always exists. However, it regresses as evaporation proceeds. At the beginning of evaporation ($t = 0.1$ ns), the calculated density of the n-dodecane liquid core was 700 kg/m^3, which is close to the experimental value of 697.54 kg/m^3 at $T = 363$ K [49]. The density in the liquid core decreases gradually because the liquid fuel is being heated up by the ambient. But after $t = 15$ ns, the evaporation enters a steady state with nearly constant liquid-core temperature. The density in the liquid core is also nearly constant. The surface and core temperatures both increase during the heat-up stage, whereas they

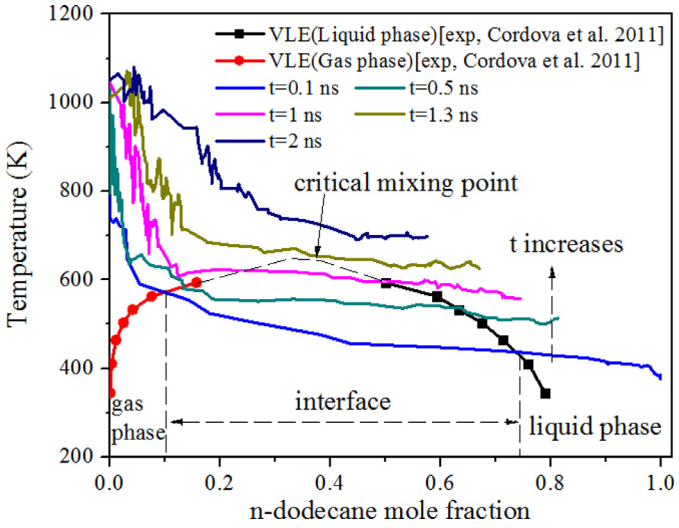

Fig. 6. The development of gas–liquid interface shown on the temperature – mole fraction VLE diagram at 20 MPa (VLE exp data: [43]).

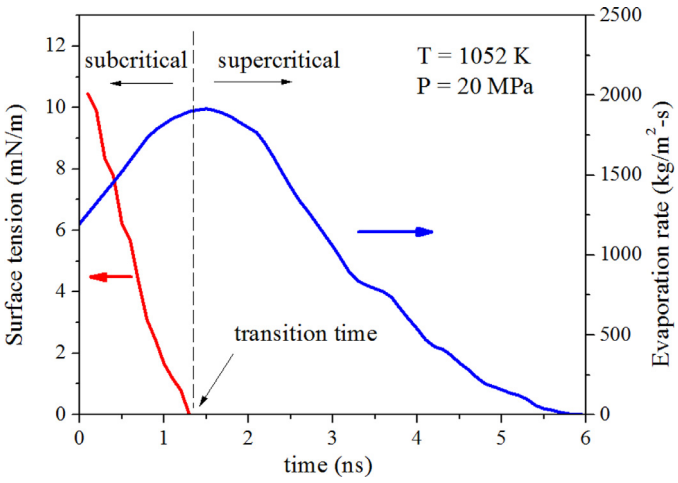

Fig. 7. The histories of surface tension and evaporation rate.

keep nearly constant during the steady-state evaporation stage. The evaporation rate remains nearly constant during the steady-state evaporation stage, about 225 kg/m^2-s. Several studies have shown that the evaporation rate of a nano-sized film (or droplet) is much higher than that of a micron- or millimeter-sized film (or droplet). For example, Yan et al. found the evaporation rate of a micron-sized (30 μm) liquid film to be around O(1) kg/m^2-s [50]. Evaporation rate of a nanoscale liquid film (1–10 nm), however, is much faster on the order of O(10)–O(100) kg/m^2-s [51–53]. This is due to the Knudsen number effect which was discussed in detail in Ref. [54]. For nano-sized liquid, for which the liquid size is smaller than the mean free path of the escaping molecules, the kinetic theory of gases, rather than continuum theory, should be used to estimate the evaporation rate [55]. Although a direct comparison of the evaporation rate between small and large droplets are less feasible, a scaling law can be applied to filter out the effect of system size. This scaling law will be discussed in detail in the following sections.

3.2. Supercritical evaporation

Here, we discuss a case of n-dodecane with an initial film thickness of $L_x = 10$ nm vaporizing into nitrogen with an ambient temperature of 1052 K and pressure of 20 MPa. We focus on how the interface evolves during the evaporation/mixing process. The results are shown in Fig. 6. The vapor–liquid equilibrium (VLE) lines for n-dodecane/nitrogen mixture at 20 MPa were obtained experimentally by Cordova et al. [43]. The critical mixing temperature at 20 MPa is the temperature at the merging point of the VLE gas phase line and the VLE liquid phase line. Note that Cordova et al. [43] obtained no data in the region near the critical point; the dashed line connecting the two VLE lines are drawn by the authors to indicate the critical temperature and mixture composition at a fixed pressure of 20 MPa.

Some background is presented here: Unlike pure species, which have a fixed critical point, the critical point for mixtures varies with mixture composition. According to the classical theory of Kiran and Levelt Sengers [56], n-dodecane/nitrogen mixtures are a TYPE IV mixture, for which the critical temperature of the mixture is lower (and higher) than the higher (and lower) critical temperature of the two components, whereas the critical pressure of the mixture is higher than the critical pressure of either component. In Fig. 6, the temperature was plotted against the mole fraction of n-dodecane (similar to Fig. 3), which may or may not intersect with the VLE lines. At $t = 0.1$ ns, the VLE lines and the temperature profile curve have two intersections. The left intersection defines the outer boundary of the interface (next to the ambient gas), and the right one defines the inner boundary of the interface (next to the liquid core). The mole fraction of n-dodecane at these two boundaries is 0.1 and 0.75, respectively. At $t = 0.5$ ns, intersections between the temperature profile and the VLE lines still exist. However, the mole fraction of n-dodecane at the outer boundary of the interface increases slightly to 0.13, but its value at the inner boundary decreases to about 0.62. The gas/liquid interface exists until $t = 1.3$ ns, indicating that the evaporation is subcritical when $t < 1.3$ ns. The temperature within the interface is always below the critical mixing temperature in this period. After $t = 1.3$ ns, the temperature profile goes above the VLE lines and exceeds the critical mixing temperature. From now on, the interface disappears and evaporation enters a diffusion-controlled mixing process, indicating that the system has become one-phase in nature.

Such a transition from two-phase evaporation to diffusion-controlled one-phase mixing is also reflected by the histories of surface tension and evaporation (or mixing) rate, as shown in Fig. 7. Initially the liquid has a surface tension of 10.5 mN/m at $t = 0.1$ ns. It decreases rapidly and eventually vanishes at $t = 1.3$ ns. The transition time based on surface tension history is consistent with the value obtained from the interface evolution history in Fig. 6. After $t = 1.3$ ns, diffusion-dominated mixing is established. The evaporation rate increases in the subcritical stage and then reaches maximum, after which the evaporation transits to supercritical. In the supercritical stage, the evaporation rate decreases, mainly because the density gradient between the liquid core and the ambient decreases over time, as shown in Fig. 7. Since the gas-liquid interface disappears after 1.3 ns, it is impossible to distinguish the liquid core and the ambient gas. Efforts were made to quantitatively describe the evaporation/mixing rate under various conditions. When evaporation enters a diffusion-dominated regime, the rate of mixing would depend on the diffusion coefficient, mass fraction gradient, and temperature gradient. In this situation, temperature gradient vanishes more quickly than concentration gradient will, so thermal diffusion effect is less prominent.

Here, we define a dimensionless transition time (τ_T) by normalizing the actual transition time (t_T) with respect to the liquid lifetime (t_L) as $\tau_T = t_T/t_L$. It characterizes how fast evaporation transits from subcritical to supercritical in the liquid's lifetime. In this supercritical evaporation case, the dimensionless transition time is

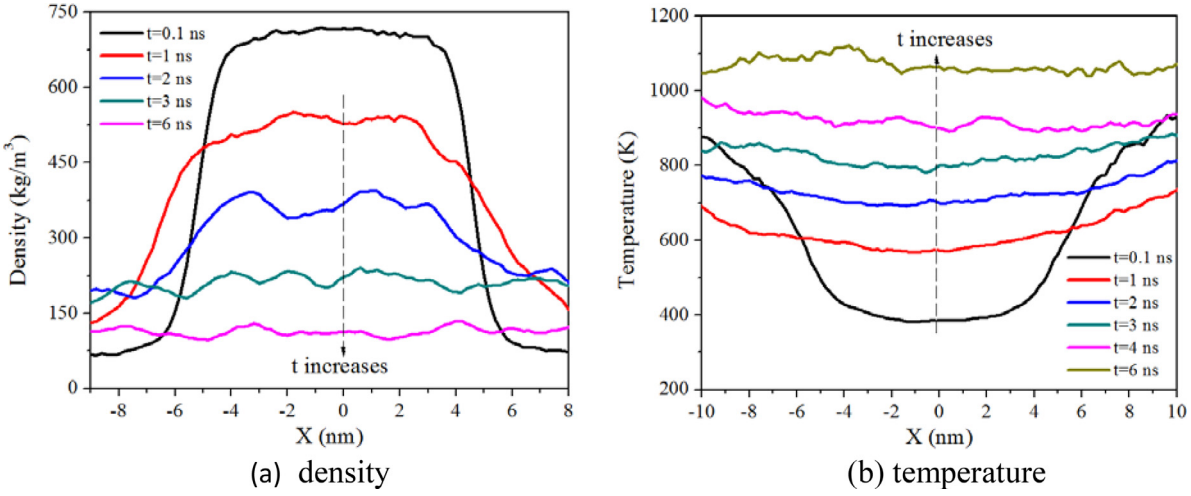

Fig. 8. The spatial distribution of mixture density and temperature as a function of time.

0.24, indicating that 24% of its lifetime is in subcritical regime and the rest in supercritical.

The mole fraction of n-dodecane in the liquid core decreases rapidly over time, which indicates that a significant amount of nitrogen has penetrated into the liquid interior and solubility effect becomes prominent at supercritical conditions. Figure 8(a) shows the spatial distribution of density as a function of time. The density of the liquid core decreases rapidly. The density gradient between the liquid core and the ambient gas becomes smaller over time. In other words, the interface is disappearing, and it is becoming more difficult to distinguish between liquid versus gas. This is the "miscible" behavior that has been observed in high-pressure injection experiments [10]. In contrast, in subcritical conditions the liquid core density is constant after steady evaporation has been established, and a sharp difference between densities of the liquid core and the ambient gas always exist until evaporation ends. Figure 8(b) shows the temperature history of the system. The liquid-core temperature continues to increase throughout the evaporation process. At $t = 2$ ns, the liquid core temperature has exceeded the critical temperature of n-dodecane of 658 K. The temperature gradient between core and ambient becomes smaller over time as the liquid core is being heated continuously. These observations are consistent with those of Kaltz et al. [26].

3.3. The scaling law: effect of liquid film size

The challenge of MD simulations is that they are computationally expensive. The time and length scales in MD studies are usually limited to a few hundred nanoseconds and nanometers, respectively. Thus the possibility of a scaling law must be explored so that the results from the MD simulations of a nanoscale system can be useful in presenting the physics of large-scale systems. This section discusses the effect of n-dodecane liquid film size on the evaporation characteristics, particularly on the normalized lifetime (τ_L/L') and the dimensionless transition time (τ_T). Three film thicknesses ($L_x = 5$, 10, and 20 nm) were considered at two different temperatures (658 and 1052 K) and various pressures (2.5–20 MPa). L_y and L_z were kept unchanged.

The liquid lifetime is determined from the beginning until the evaporation or mixing rate approaches zero with a nearly uniform distribution of density, species concentration, and temperature within the initial liquid volume. We first define a dimensionless lifetime τ_L as $\tau_L = t_L/t_{L,\,ref}$, where t_L is the actual lifetime of the liquid film and $t_{L,\,ref}$ is the lifetime of a reference film. The reference film was chosen to have a given initial thickness $L_{ref} = 5$ nm, ambient temperature $T_{ref} = 658$ K, and pressure $P_{ref} = 2.5$ MPa. With respect to the reference quantities, we obtain dimensionless temperature, pressure and thickness as $T' = T/T_{ref}$, $P' = P/P_{ref}$, and $L' = L/L_{ref}$. The dimensionless lifetime τ_L is then normalized by L' with hopes to filter out the effect of system size (film thickness).

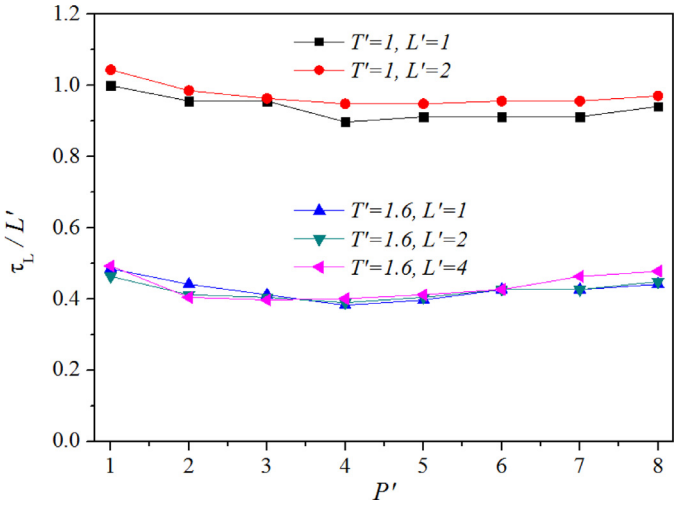

Fig. 9. The normalized liquid film lifetime as a function of normalized ambient temperature, pressure and film thickness. The reference condition is at $T_{ref} = 658$ K, $P_{ref} = 2.5$ MPa, and $L_{ref} = 5$ nm.

Figure 9 presents the normalized lifetime τ_L/L' for n-dodecane liquid film at various normalized ambient temperatures T' and pressures P' and for three normalized thicknesses L'. The results show that τ_L/L' has a strong dependence on the ambient temperature – higher T' results in lower values of τ_L. It also depends on the ambient pressure, although the dependence is less prominent than the temperature. Furthermore, the dimensionless lifetime τ_L is proportional to the liquid film thickness L. After being normalized by the thickness ratio L', τ_L is nearly identical for three thicknesses under a given ambient temperature and pressure, indicating that a scaling law indeed exists.

Next we look at how the dimensionless transition time depends on system size. It is desirable to know at what conditions and when the transition from subcritical evaporation to diffusion-controlled supercritical mixing will occur. This is because the theoretical framework of these two regimes is quite different (two-phase models plus interface equilibrium vs. one-phase models).

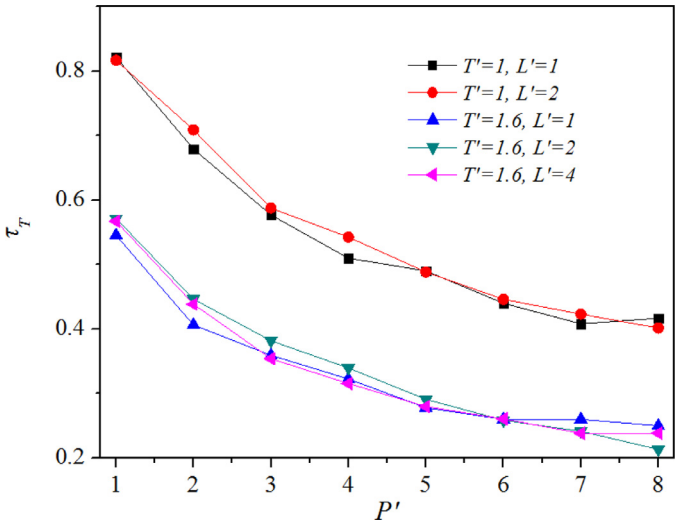

Fig 10. The dimensionless transition time as a function of normalized ambient temperature, pressure and film thickness. The reference condition is at T_{ref} = 658 K, P_{ref} = 2.5 MPa, and L_{ref} = 5 nm.

Figure 10 shows the dimensionless transition time for n-dodecane liquid film as a function of dimensionless ambient temperature, pressure, and film thickness. Note that τ_T is defined as the ratio of the actual transition time (t_T) with respect to the liquid lifetime (t_L) as $\tau_T = t_T/t_L$. The results show that τ_T is independent of the dimensionless thickness, indicating that the results can be used to approximate transition from subcritical to supercritical in macroscopic systems. The transition time, however, has a strong dependence on the ambient temperature and pressure. With increasing ambient temperature and pressure, transition to supercritical occurs earlier. This is discussed in the following section.

The scaling law is not surprising, however, because evaporation is a surface phenomenon – it is the surface elements that are responsible for phase change, and the interface dynamics play an important role in such phenomenon. Note Dahms and Oefelein [17] predicted the thickness of the interface varies from 0.9 to 2.6 nm under a wide range of temperatures and pressures. Previous studies have indeed confirmed that some evaporation characteristics are size-independent. For example, Harstad and Bellan [57,58] simulated evaporation of millimeter-sized heptane droplets into nitrogen and found the variation of D-square with scaled time is independent of droplet size under both subcritical and supercritical pressures. Yang et al. [59] simulated micron-sized liquid oxygen droplets vaporizing into hydrogen and found the calculated droplet lifetime varies linearly with the square of the initial droplet diameter for different droplet sizes. Furthermore, Oefelein and Aggarwal demonstrated in their DNS simulations that the minimum pressure required for droplet surface to reach its critical mixing state is size-independent [11].

3.4. Effects of ambient temperature and pressure on the transition

Next, we will focus on how long does it take to transit to supercritical, from subcritical, and how the transition time depends on fuel type and ambient conditions. The dimensionless transition time τ_T was calculated for various ambient temperatures and pressures for a liquid film with a thickness of 10 nm for n-heptane, n-dodecane and n-hexadecane. The contours of constant τ_T were plotted as functions of ambient temperature and pressure, as shown in Fig. 11 for the three fuels. In general, τ_T decreases with increasing pressure and temperature. This is because higher ambient pressure and temperature lead to stronger gas solubility and heat transfer into the liquid core, which promotes the interface to approach the critical mixing point faster.

Table 2
Correlation parameters of dimensionless transition time for three alkanes.

	n-Heptane	n-Dodecane	n-Hexadecane
a_1	− 0.40211	− 0.49085	− 0.53209
a_2	0.21282	0.35460	0.46148
a_3	− 0.04160	− 0.07587	− 0.12921
b_1	− 0.00230	0.02353	0.00406
b_2	0.05711	0.00661	0.01410
b_3	− 0.01638	− 0.00713	− 0.00219
Conditions	$1 \le T_r \le 2.4$	$1 \le T_r \le 2$	$1 \le T_r \le 1.8$
	$1 \le P_r \le 7.3$	$1 \le P_r \le 11$	$1 \le P_r \le 14.3$

Crua et al. [10] recently investigated the injection of three liquid fuels (n-heptane, n-dodecane, and n-hexadecane) into high temperature and pressure ambient gases made of H_2O, CO_2, and N_2, using a constant-volume preburn combustion vessel. They found that the time taken by a droplet to transition to miscible mixing depends on the fuel properties and the ambient temperature and pressure. Using high-speed and high-resolution microscopic visualizations, they developed a pressure-temperature diagram on which each test condition was marked for whether classical evaporation was observed or droplet deformation and significant miscible mixing was observed. We marked each case (the corresponding ambient temperature and pressure) for which they observed either classical droplet evaporation (open circles) or strong miscible mixing behavior (black dots) in our diagram in Fig. 11. For example, for n-dodecane in Fig. 11(b), almost all black dots fall within the area where $\tau_T < 0.35$, indicating that for those cases more than 65 percent of the liquid lifetime experiences supercritical mixing. All open circles fall within the area where $\tau_T > 0.35$, indicating that the liquid experiences subcritical evaporation for more than 35 percent of its lifetime. Thus it is reasonable to infer that subcritical evaporation dominates when $\tau_T > 0.35$, but diffusion-controlled supercritical mixing dominates when $\tau_T < 0.35$ for n-dodecane. For n-heptane and n-hexadecane, the dimensionless transition time isolines $\tau_T = 0.35$ also separate the significant miscible mixing behavior from the classical droplet evaporation as observed in [10].

Based on the experimental data, we may use a threshold of $\tau_T = 0.35$ to separate the subcritical-dominated and supercritical-dominated evaporation regimes on the P-T diagram for n-alkanes (C_7 – C_{16}). Note if the ambient temperature and pressure are not high enough, the liquid will experience subcritical evaporation for most of its lifetime. For example, according to Fig. 11(b), to have $\tau_T < 0.35$, an ambient temperature of 900 K would require the ambient pressure to be higher than 8 MPa and an ambient temperature of 1000 K would require the ambient pressure to be higher than 6.5 MPa. Thus for low ambient pressures, which, however, are still above the critical pressure of the injected fuel, surface tension exists and dominates the evaporation and mixing processes for most of the liquid's lifetime; supercritical mixing will occur only in its later life, which may be undetectable by optical diagnostics because of the small length and time scales of the second stage. This might be the reason that Lazar and Faeth [60] proposed the critical mixing pressure required for supercritical burning of n-octane or n-decane in air to be 2–2.5 times of the critical pressure of the pure hydrocarbon.

We have discovered that the dimensionless transition time τ_T is independent of the liquid film size, but that it has a strong dependence on the ambient temperature and pressure. By fitting a series of MD simulation results, we developed empirical correlations to describe such dependence. Table 2 summarizes the parameters and the conditions of the correlations for n-heptane, n-dodecane

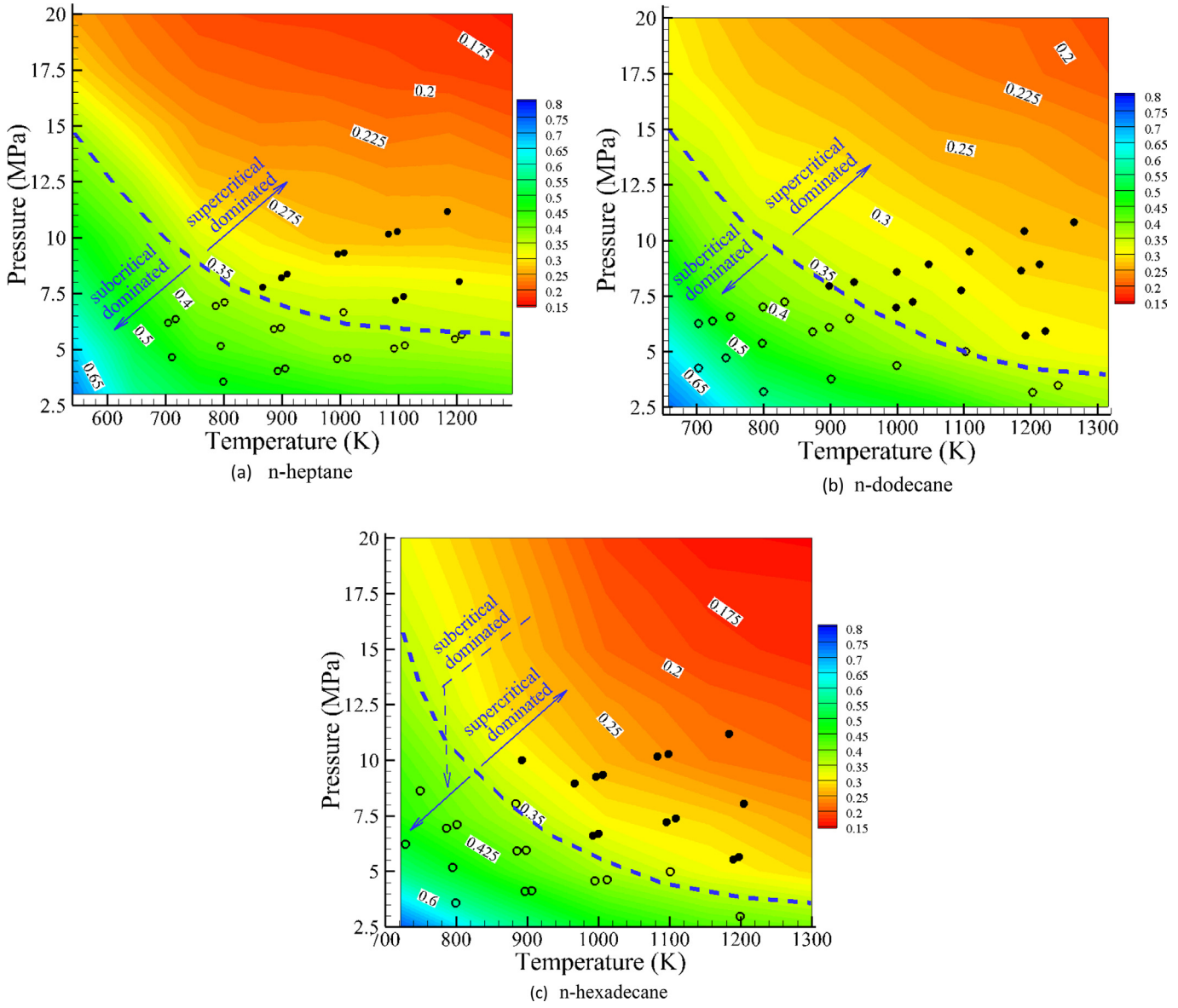

Fig. 11. Contours of dimensionless transition time on pressure-temperature diagrams for n-heptane (a), n-dodecane (b) and n-hexadecane (c). Blue dashed lines indicate the contours of $\tau_T = 0.35$. The open circles represent conditions at which significant droplet deformation and miscible mixing were observed, whereas the circle dots represent conditions at which classical evaporation was be observed, according to Crua et al. [10].

and n-hexadecane, respectively.

$$\tau_T = \frac{t_T}{t_L} = a * \ln\left[b * \left(\frac{P}{P_C}\right)\right] \tag{10}$$

$$a = \left(\mathrm{a1} + \mathrm{a2} * T_r + \mathrm{a3} * T_r^2\right)$$
$$b = \left(\mathrm{b1} + \mathrm{b2} * T_r + \mathrm{b3} * T_r^2\right)$$
$$\left(T_r = \frac{T}{T_C}, \quad P_r = \frac{P}{P_C}\right)$$

where T_r and P_r are the reduced temperature and pressure of liquid fuel. This equation is for $T_r > 1$ and $P_r > 1$. The correlations provide a convenient means of estimating the pressure and temperature dependence of the transition time under supercritical conditions. The fitting error is acceptable as the root-mean-square-error (RMSE) of dimensionless transition time is smaller than 0.021.

3.5. Effect of ambient temperature and pressure on liquid lifetime

Here, we will examine the effects of ambient pressure and temperature on the lifetime of the n-dodecane liquid film. The results are shown in Fig. 12. The dashed line, which represents a value of 0.35 for the dimensionless transition time, divides the diagram into two regions. The left region is subcritical-dominated, meaning that the liquid experiences subcritical evaporation for most of its lifetime. The right region is supercritical-dominated in the sense that more than half of the liquid lifetime is a diffusion-controlled, one-phase mixing process. In the subcritical-dominated region, the lifetime decreases as the pressure increases, mainly because the enthalpy of evaporation reduces as pressure increases. In the supercritical-dominated region, the pressure effect was reversed resulting in a slightly increased lifetime. This is because evaporation has become diffusion-controlled; increasing pressure reduces binary mass diffusivity, although the degree of reduction of mass diffusivity is much less prominent at higher pressures than at low pressures [61], which is why only a slight increase in the

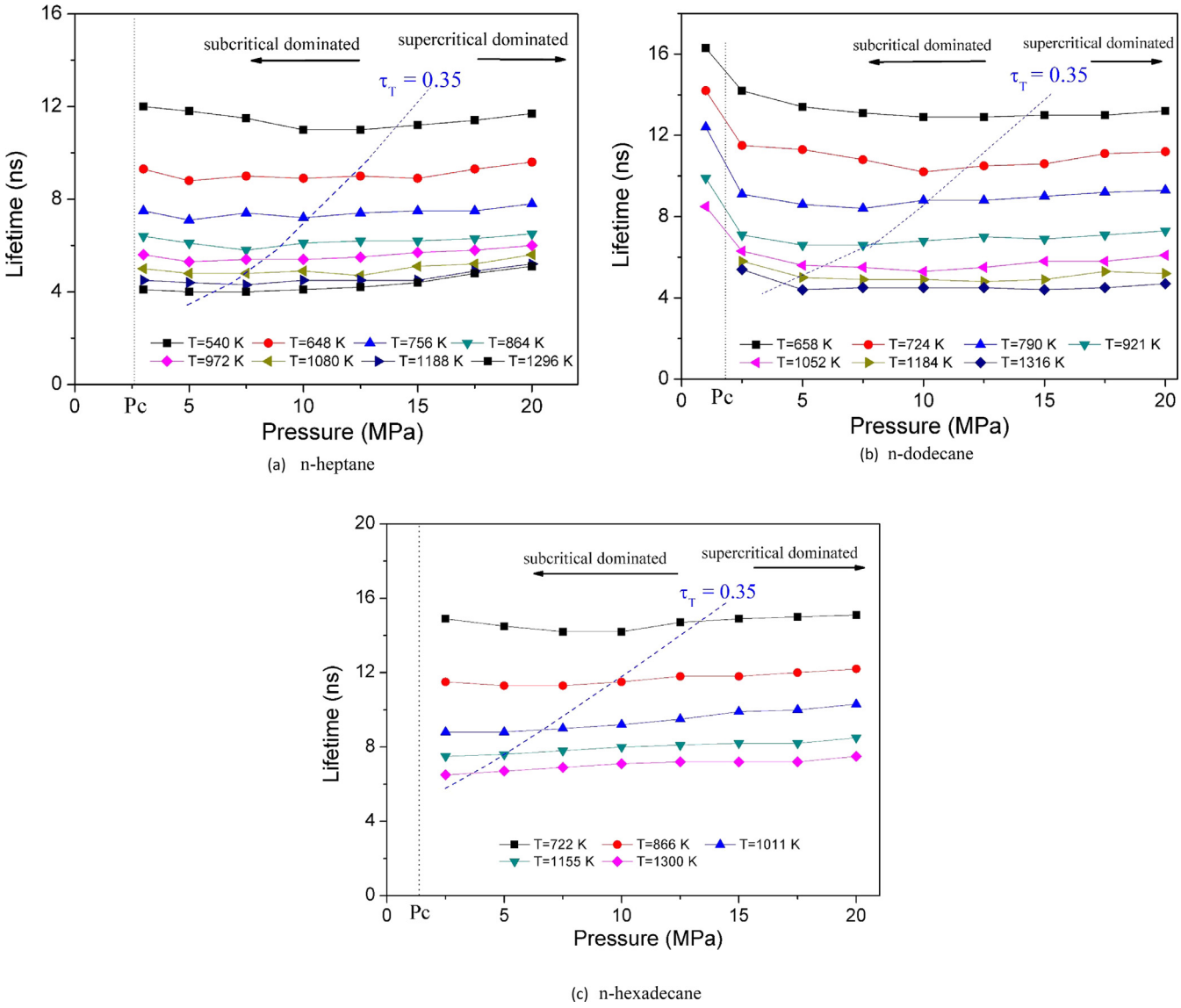

Fig. 12. The liquid lifetime as a function of ambient temperature and pressure for the three fuels. The dashed line represents $\tau_T = 0.35$. The dotted vertical line indicates the critical pressure of the liquid fuel.

lifetime at high pressures was observed in Fig. 12. The trend of pressure dependence agrees with the detailed numerical simulations of liquid oxygen droplets vaporizing into hydrogen by Yang et al. [59] and the measurements of n-heptane droplet evaporation into nitrogen at high pressures by Sato [62].

3.6. Comparison of transition for three n-alkane fuels

Figure 13 shows the subcritical-dominated and supercritical-dominated regimes for n-heptane, n-dodecane and n-hexadecane on the P-T diagram. The transition lines that separate the two regimes were obtained from the isolines of $\tau_T = 0.35$. Here, we chose 0.35 for τ_T simply because the experiment of Crua et al. [10] suggests this value. Nevertheless, theoretically speaking, a value of 0.5 would be more appropriate to define the two regimes. The results in Fig. 13 show that the three alkanes exhibit similar shape. The reduced pressure required for transition increases with carbon number in the alkanes. For all three fuels, when the reduced temperature is smaller than 1.5, the reduced pressure decreases rapidly with increasing reduced temperature. However, when the reduced temperature is larger than 1.5, the reduced pressure decreased slowly. This same trend was also observed in the detailed thermodynamics analysis of Dahms and Oefelein [16] which used the Knudsen number of the gas/liquid interface to separate different regimes. However, the present transition lines obtained using $\tau_T = 0.35$ as the criterion to separate the two regimes are higher than those of Dahms and Oefelein [16] which were obtained based on a threshold Knudsen number of the interface $Kn = 0.1$.

4. Conclusions

MD simulations were conducted to understand the transition from classical two-phase evaporation to diffusion-controlled one-phase mixing for three n-alkanes fuels vaporizing into nitrogen under various ambient temperatures and pressures. The dimensionless transition time is independent of the liquid film thickness, but has a strong dependence on the ambient temperature and pressure. With increasing ambient temperature and pressure, transition from subcritical to supercritical occurs earlier. Correlations were proposed to describe the dimensionless transition time as a function of ambient temperature and pressure for n-heptane,

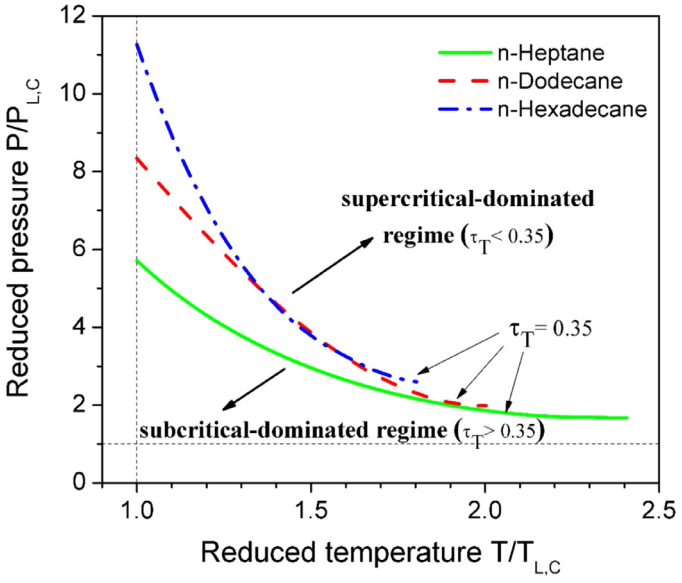

Fig. 13. Subcritical-dominated and supercritical-dominated regimes on the P-T diagram, which are separated by a dimensionless transition time of 0.35 for three different n-alkanes. $T_{L,initial} = 363$ K.

n-dodecane and n-hexadecane. A threshold of the dimensionless transition time of 0.35 may be used to separate two regimes: subcritical-dominated and supercritical-dominated regimes. Also, the normalized liquid film lifetime is independent of the liquid film thickness. It decreases as the pressure increases in the subcritical-dominated region due to the reduced enthalpy of evaporation at higher pressures. In supercritical-dominated region, the pressure effect was reversed leading to slightly increased lifetime because of the slightly reduced binary mass diffusivity at higher pressures.

Acknowledgment

This research was supported by the Air Force Office of Scientific Research (AFOSR) with Dr. Chiping Li as the technical monitor.

References

[1] V. Yang, Modeling of supercritical vaporization, mixing, and combustion processes in liquid-fueled propulsion systems, Proc. Combust. Inst. 28 (2000) 925–942.
[2] S.D. Givler, J. Abraham, Supercritical droplet vaporization and combustion studies, Prog. Energy Combust. Sci. 22 (1996) 1–28.
[3] J. Bellan, Supercritical (and subcritical) fluid behavior and modeling: drops, streams, shear and mixing layers, jets and sprays, Prog. Energy Combust. Sci. 26 (2000) 329–366.
[4] W.O.H. Mayer, A.H.A. Schik, Atomization and breakup of cryogenic propellants under high-pressure subcritical and supercritical conditions, J. Prop. Power 14 (5) (1998) 835–842.
[5] C. Segal, S.A. Polikhov, Subcritical to supercritical mixing, Phys. fluids 20 (2008) 052101.
[6] R.R. Rachedi, L.C. Crook, P.E. Sojka, An experimental study of swirling supercritical hydrocarbon fuel jets, J. Eng. Gas Turb. Power 132 (2010) 081502.
[7] B. Chehroudi, Recent experimental efforts on high-pressure supercritical injection for liquid rockets and their implications, Int. J. Aerosp. Eng. (2012) Article ID 121802.
[8] M. Oschwald, J.J. Smith, R. Branam, J. Hussong, A. Schik, B. Chehroudi, D. Talley, Injection of fluids into supercritical environments, Combust. Sci. Technol. 178 (2006) 49–100.
[9] J. Manin, M. Bardi, L.M. Pickett, R.N. Dahms, J.C. Oefelein, Microscopic investigation of the atomization and mixing processes of diesel sprays injected into high pressure and temperature, Fuel 134 (2014) 531–543.
[10] C. Crua, J. Manin, L.M. Pickett, Transition from droplet evaporation to miscible mixing at diesel engine conditions, 13th Triennial International Conference on Liquid Atomization and Spray Systems, Taiwan (2015).
[11] J.C. Oefelein, S.K. Aggarwal, Toward a unified high-pressure drop model for spray simulations, Proceedings of the Summer Program, Center for Turbulence Research (2000), pp. 193–206.
[12] G.S. Zhu, S.K. Aggarwal, Transient supercritical droplet evaporation with emphasis on the effects of equation of state, Int. J. Heat Mass Transf. 43 (2000) 1157–1171.
[13] G. Zhu, R.D. Reitz, S.K. Agarwal, Gas-phase unsteadiness and its influence on droplet vaporization in sub- and super-critical environments, Int. J. Heat Mass Transf. 44 (16) (2001) 3081–3093.
[14] G. Zhu, R.D. Reitz, A model for high-pressure vaporization of droplets of complex liquid mixtures using continuous thermodynamics, Int. J. Heat Mass Transf. 45 (2002) 495–507.
[15] R.N. Dahms, J. Manin, L.M. Pickett, J.C. Oefelein, Understanding high-pressure gas-liquid interface phenomena in diesel engines, Proc. Combust. Inst. 34 (1) (2013) 1667–1675.
[16] R.N. Dahms, J.C. Oefelein, Liquid jet breakup regimes at supercritical pressures, Combust. Flame 162 (2015) 3648–3657.
[17] R.N. Dahms, J.C. Oefelein, On the transition between two-phase and single-phase interface dynamics in multicomponent fluids at supercritical pressures, Phys. Fluids 25 (2013) 092103.
[18] R.N. Dahms, J.C. Oefelein, Atomization and dense-fluid breakup regimes in liquid rocket engines, J. Propuls. Power 31 (5) (2015) 1221–1231.
[19] A.I. Rusanov, E.N. Brodskaya, The molecular dynamics simulation of a small drop, J. Colloid Interface Sci. 62 (3) (1977) 542–556.
[20] S.M. Thompson, K.E. Gubbins, A molecular dynamics study of liquid drops, J. Chem. Phys. 81 (1) (1984) 530–544.
[21] S. Maruyama, S. Matsumoto, A. Ogita, Surface phenomena of molecular clusters by molecular dynamics method, Therm. Sci. Eng. 2 (1) (1994) 78–84.
[22] R.S. Dumont, S. Jain, A.G. Basile, Argon cluster evaporation dynamics, J. Chem. Phys. 10 (1995) 102.
[23] C.J. Ohlandt, Molecular dynamics simulation of argon droplet evap oration with three body force potentials (Thesis), Pennsylvania State University, 1996.
[24] J.K. Little, Simulation of droplet evaporation in supercritical environments using parallel molecular dynamics (Dissertation), Pennsylvania State University, 1996.
[25] L.N. Long, M.M. Micci, B.C. Wong, Molecular dynamics simulations of droplet evaporation, Comput. Phys. Commun. 96 (2–3) (1996) 167–172.
[26] T.L. Kaltz, L.N. Long, M.M. Micci, J.K. Little, Supercritical vaporization of liquid oxygen droplets using molecular dynamics, Combust. Sci. Tech. 136 (1998) 279–301.
[27] A.P. Bhansali, Y. Bayazitoglu, S. Maruyama, Molecular dynamics simulation of an evaporating sodium droplet, Int. J. Therm. Sci. 38 (1999) 66–74.
[28] J.H. Walther, P. Koumoutsakos, Molecular dynamics simulation of nanodroplet evaporation, J. Heat Transf. 123 (2001) 741–748.
[29] P. Yi, D. Poulikakos, J. Walther, G. Yadigaroglu, Molecular dynamics simulation of vaporization of an ultra-thin liquid argon layer on a surface, Int. J. Heat Mass transf. 45 (2002) 2087–2100.
[30] L. Consolini, S.K. Aggarwal, S. Murad, A molecular dynamics simulation of droplet evaporation, Int. J. Heat Mass Transf. 46 (2003) 3179–3188.
[31] S. Sumardiono, J. Fischer, Molecular simulations of droplet evaporation processes: adiabatic pressure jump evaporation, Int. J. Heat Mass Transf. 49 (2006) 1148–1161.
[32] S. Sumardiono, J. Fischer, Molecular simulations of droplet evaporation by heat transfer, Microfluid. Nanofluid. 3 (2007) 127–140.
[33] E.S. Landry, S. Mikkilineni, M. Paharia, A.J.H. McGaughey, Droplet evaporation: a molecular dynamics investigation, J. Appl. Phys 102 (2007) 124301.
[34] S. Cheng, J.B. Lechman, S.J. Plimpton, G.S. Grest, Evaporation of Lennard-Jones fluids, J. Chem. Phys. 134 (2011) 224704.
[35] B.A. Petrilla, M.F. Trujillo, M.M. Micci, n-Heptane droplet vaporization using molecular dynamics, Atomization and Sprays 20 (7) (2010) 581–593.
[36] J. Xie, S.S. Sazhin, B. Cao, Molecular dynamics study of the processes in the vicinity of the n-dodecane vapour/liquid interface, Phys. Fluids 23 (2011) 112104.
[37] J. Xie, S.S. Sazhin, B. Cao, Molecular dynamics study of condensation/evaporation and velocity distribution of n-dodecane at liquid-vapour phase equilibri, J. Therm. Sci. Tech. 7 (2012) 288–301.
[38] M.G. Martin, J.I. Siepmann, Transferable potentials for phase equilibria. 1. United-atom description of n-alkanes, J. Phys. Chem. B 102 (1998) 2569–2577.
[39] B. Smit, S. Karaborni, J.I. Siepmann, Computer simulations of vapor–liquid phase equilibria of n-alkanes, J. Chem. Phys. 102 (1995) 2126–2140.
[40] S.K. Nath, F.A. Escobedo, J.J. de Pabloa, On the simulation of vapor±liquid equilibria for alkanes, J. Chem. Phys. 108 (23) (1998) 9905–9911.
[41] W.L. Jorgensen, J.D. Madura, C.J. Swenson, Optimized intermolecular potential functions for liquid hydrocarbon, J. Am. Chem. Soc. 106 (1984) 6638–6646.
[42] G. Mo, L. Qiao, Monte Carlo simulations using various potentials for vapor-liquid equilibrium of n-alkane and nitrogen mixtures under high pressure, 2016, in preparation.
[43] T.G. Cordova, D.N. Justo-García, B.E. García-Flores, F. García-Sanchez, Vapor-liquid equilibrium data for the nitrogen and dodecane system at temperatures from (344 to 593) K and at pressures up to 60 MPa, J. Chem. Eng. Data 56 (2011) 1555–1564.
[44] J.L. Rivera, J. Alejandre, Vapor–liquid equilibrium simulations of nitrogen and n-alkane binary mixtures, Colloids Surf., A 207 (2002) 223–228.
[45] J.P.R.B. Walton, D.J. Tildesley, J.S. Rowlinson, J.R. Henderson, The pressure tensor at the planar surface of a liquid, Mol. Phys. 48 (6) (1983) 1357–1368.
[46] S. Plimpton, Fast parallel algorithms for short-range molecular dynamics, J. Comput. Phys. 117 (1995) 1–19.
[47] D.V.D. Spoel, E. Lindahl, B. Hess, G. Groenhof, A.E. Mark, H.J.C. Berendsen, Gromacs: fast, flexible, and free, J. Comput. Chem. 26 (16) (2005) 1701–1718.

[48] J.H. Irving, J.G. Kirkwood, The statistical mechanical theory of transport processes. IV. The equations of hydrodynamics, J. Chem. Phys. 18 (1950) 817–829.
[49] National institute of standards and technology, Dodecane chemistry, 2016. http://webbook.nist.gov/cgi/cbook.cgi?ID=C112403&Units=SI.
[50] Y. Yan, H. Liu, M. Jia, M. Xie, H. Yin, A one-dimensional unsteady wall film evaporation model, Int. J. Heat Mass Transf. 88 (2015) 138–148.
[51] G. Nagayama, M. Kawagoe, A. Tokunaga, T. Tsuruta, On the evaporation rate of ultra-thin liquid film at the nanostructured surface: A molecular dynamics study, Int. J. Therm. Sci. 49 (2010) 59–66.
[52] J. Yu, H. Wang, A molecular dynamics investigation on evaporation of thin liquid films, Int. J. Heat Mass Transf. 55 (2012) 1218–1225.
[53] A.K.M.M. Morshed, T.C. Paul, J.A. Khan, Effect of nanostructures on evaporation and explosive boiling of thin liquid films: a molecular dynamics study, Appl. Phys. A 105 (2011) 445–451.
[54] E.J. Davis, A.K. Ray, Submicron droplet evaporation in the continuum and non–continuum regimes, J. Aerosol Sci. 9 (1978) 411–422.
[55] R. Chang, E.J. Davis, Knudsen aerosol evaporation, J. Colloid Interface Sci. 54 (3) (1976) 352–364.
[56] E. Kiran, J.M.H. Levelt Sengers, Supercritical fluids: fundamentals for application, Kluwer Academic Publishers: Dordrecht, 1994.
[57] K. Harstad, J. Bellan, An all-pressure fluid drop model applied to a binary mixture: heptanes in nitrogen, Int. J. Multiph. Flow 26 (2000) 1675–1706.
[58] K. Harstad, J. Bellan, Evaluation of commonly used assumptions for isolated and cluster heptane drops in nitrogen at all Pressures, Combust. Flame 127 (2001) 1861–1879.
[59] V. Yang, N. Lin, J. Shuen, Vaporization of liquid oxygen (LOX) droplets in supercritical hydrogen environments, Combust. Sci. Tech. 97 (1994) 247–270.
[60] R.S. Lazar, G.M. Faeth, Bipropellant droplet combustion in the vicinity of the critical point, Symp. (Int.) Combust. 13 (1971) 801–811.
[61] Y. Zhu, X. Lu, J. Zhou, Y. Wang, J. Shi, Prediction of diffusion coefficients for gas, liquid and supercritical fluid: application to pure real fluids and infinite dilute binary solutions based on the simulation of Lennard–Jones fluid, Fluid Phase Equilibria 194–197 (2002) 1141–1159.
[62] J. Sato, Studies on droplet evaporation and combustion in high pressures, 31st Aerospace Science Meeting & Exhibit, AIAA 93-0813, Reno NV (1993).